IEEE Access
Multidisciplinary | Rapid Review | Open Access Journal

Received January 4, 2021, accepted January 23, 2021, date of publication January 27, 2021, date of current version February 3, 2021.

Digital Object Identifier 10.1109/ACCESS.2021.3054899

Sand-Dust Image Enhancement Using Successive Color Balance With Coincident Chromatic Histogram

TAE HEE PARK[1] AND IL KYU EOM[2]
[1]Department of Mechatronics Engineering, Tongmyong University, Busan 48520, South Korea
[2]Department of Electronics Engineering, Pusan National University, Busan 46241, South Korea

Corresponding author: Il Kyu Eom (ikeom@pusan.ac.kr)

This work was supported by the Tongmyong University Research Grants under Grant 2019A017.

ABSTRACT Outdoor images in sand-dust environments play an adverse role in various remote-based computer vision tasks because captured sand-dust images have severe color casts, low contrast, and poor visibility. However, although sand-dust image restoration is as important as haze removal and underwater image enhancement, it has not been sufficiently studied. In this paper, we present a novel color balance algorithm for sand-dust image enhancement. The aim of the proposed enhancement method is to obtain a coincident chromatic histogram. First, we introduce a pixel-adaptive color correction method using the mean and standard deviation of chromatic histograms. Pixels of each color component are adjusted based on the statistical characteristics of the green component. Second, a green-mean-preserving color normalization technique is presented. However, using the mean of red and blue components as the mean of the green can result in an undesirable output because the red or blue components of many sand-dust images have a narrow histogram with a high peak. To address this problem, we propose a histogram shifting algorithm that makes the red and blue histograms overlap the green histogram as much as possible. Based on this algorithm, bluish or reddish artifacts of the enhanced image can be reduced. Finally, image adjustment is exploited to improve the brightness of the sand-dust image. We performed intensive experiments for various sand-dust images and compared the performance of the proposed method with those of state-of-the-art enhancement methods. The simulation results indicate that the proposed enhancement scheme outperforms the existing approaches in terms of both subjective and objective qualities.

INDEX TERMS Sand-dust image enhancement, color normalization, green-mean preserving, maximum overlapped histogram, coincident chromatic histogram.

I. INTRODUCTION

The performances of outdoor vision systems, such as intelligent surveillance systems, human and vehicle tracking systems, image-based remote monitoring systems, and traffic monitoring systems, affected by adverse atmospheric conditions. Outdoor images and videos captured in inclement weather conditions have poor contrast, color cast, low visibility, fuzz, and darkness. Haze or fog is one of the most common image quality deterioration factors caused by bad weather. Therefore, extensive studies on hazy removal [1]–[7] have been conducted. In recent decades, sand dust has been a threat to human life and health and has an adverse effect on outdoor vision applications. In sand-dust weather conditions, because blue and green light are absorbed by sand-dust particles much more quickly than red light, captured images appear yellow or even red overall. Furthermore, since the radius of sand-dust particles is much larger than that of haze and fog particles [8], direct application of the haze removal method to sand-dust image enhancement will fail. Therefore, sand-dust image enhancement can be a more challenging problem than conventional dehazing and underwater image enhancement. However, studies on sand-dust image enhancement have not been actively conducted.

The main problems of sand-dust image enhancement are severe color shifts or casts. Classical color correction-based

The associate editor coordinating the review of this manuscript and approving it for publication was Qiangqiang Yuan.

algorithms [9]–[12] are not directly applicable for adjusting the color shift or casting of sand-dust images. Therefore, various color correction approaches specialized in sand-dust weather conditions are applied to enhance images. Fu *et al.* [13] presented a fusion-based enhancing method for a single sand-dust image. In this approach, the observed image was color corrected based on a statistical strategy. By applying two different Gamma corrections to the color-corrected sand-dust image, they generated two images with different brightness levels. The enhanced image was obtained by fusing two Gamma corrected images with three weighted maps that represent sharpness, chromaticity, and prominence. The enhancement performance was reasonable for weak sand-dust conditions. However, this method failed to enhance heavy sand-dust images. Yan *et al.* [14] exploited global fuzzy enhancement [15] and band-limited histogram equalization to enhance sand-dust images. To further enhance the image details, a partially overlapped sub-block histogram equalization [16] was applied. Although the contrast of sand-dust images was improved, the overall enhancement effect was not satisfactory. Al-Ameen proposed a visibility enhancement method for sand-dust images based on tuned tri-threshold fuzzy intensification operators [17]. Fuzzy operators were applied to the captured image with a different threshold for each color channel. However, this method still showed color casts. Wang *et al.* [18] reported a sand-dust image enhancement algorithm in the Lab color space. Two chromatic components were combined to perform color cast correction and saturation stretching. Meanwhile, fast local Laplacian filtering was employed to lightness component to enhance details. However, this method generated a blueness phenomenon in the enhanced images. Recently, Shi *et al.* [19] proposed a normalized gamma transformation-based contrast-limited adaptive histogram equalization for sand-dust image enhancement in Lab color space. This method consists of contrast enhancement and color correction. The contrast of the lightness component of the sand-dust image was enhanced using contrast-limited adaptive histogram equalization [20], followed by a normalized gamma correction operation. For chromatic components, a gray-world-based color correction method was used. This algorithm generated a reasonable sand-dust image. However, the performance was poor for seriously degraded images such as red-storm images, and this method could not remove dust haze from images.

Another popular method for sand-dust image enhancement is the image restoration-based approach. This approach mainly exploits the atmospheric scattering model (ASM) [21], which is widely used in the field of haze removal. Huang *et al.* [22] introduced a visibility restoration technique based on the dark channel prior (DCP) [1]. To avoid insufficient estimation of haze thickness, a haze thickness estimation module was proposed based on Laplacian-based gamma correction, and the Laplacian-based white patch-Retinex technique was used to recover true scene colors. This algorithm produced a bluish artifact for most sand-dust images. This artifact seemed to exist because the weak blue channel and the strong red channel were not considered in ASM. Yu *et al.* [23] proposed a sand-dust degraded image restoration method based on ASM and information loss constraint, which could improve the contrast of different kinds of degraded images. This method accurately estimated the atmospheric light by iterating atmospheric light to compensate for the color shift. However, this method showed the problem of halos. Shi *et al.* [24] presented a DCP-based image enhancement algorithm based on halo elimination. The color components in the Lab color space were used to remove the color shift. In addition, the improved DCP was used to remove haze in the RGB space. Finally, the brightness component in the Lab space was stretched to enhance contrast. This method effectively improved the visibility of sand-dust images, however, the recovered colors showed a dim phenomenon. Recently, Gao *et al.* [25] proposed an ASM-based sand-dust image enhancement method based on reversing the blue channel. The atmospheric light and the transmission map were estimated using this prior. However, this approach failed to recover degraded images with a large degree of sand dust. Cheng *et al.* [26] employed a blue channel prior and a fusion method to recover sand-dust degraded images. The blue channel technology was issued to enhance image contrast, and white balancing technology was exploited to resolve the color distortion. Multilayer decomposition and multi-scale fusion technologies were employed to restore important faded features and edge information. This approach generated reasonable enhancement results. However, this method did not show results from images with severe color casts, and the computational cost was not high. Kim *et al.* [5] proposed a fast single-image dehazing method using saturation-based transmission map estimation. This algorithm also presented a color veil removing approach based on the gray-world assumption. However, this method showed a severe color cast for sand-dust images with a high degree of sand dust.

Sand-dust images have a weak blue component and a strong red component. However, most sand-dust image enhancement methods do not fully consider the characteristics of the color distributions of sand-dust images. The blue channel prior, which inverts the blue color component [25], [26], was employed in recent years. This blue channel prior can cause a bluish artifact in restored images because the inverting process of a very weak blue component produces a very strong blue color. This paper presents a novel image enhancement algorithm using the color distribution characteristics of sand-dust images. The proposed restoration method comprises four steps. In the first step, a new initial color balance method, which consists of three compensation terms, is presented. The first step employs the color histogram characteristics of sand-dust images, such as means and standard deviations. In the second step, a green-mean-preserving image normalization algorithm is proposed based on the previously corrected color channels. Most color balance techniques tend to make the red and blue means equal to the green mean. However, because the red or blue

components of many sand-dust images have a narrow histogram with a high peak, undesirable restoration results may be obtained. Therefore, this paper introduces a method of overlapping the three histograms in as many areas as possible rather than equalizing the means. In the final step, an image adjustment technique is performed to improve the brightness of the sand-dust images. The proposed method is fast and generates reasonable enhancement results in a wide variety of sand-dust images.

The remainder of this paper is organized as follows. The color distribution of a sand-dust image is examined in Section II. The proposed successive color correction algorithm is presented in Section III. Section IV presents the experimental results obtained using the proposed approach, and finally, the paper is concluded in Section V.

II. COLOR DISTRIBUTION OF SAND-DUST IMAGE

Images can be degraded due to various causes, such as lighting condition, weather, and atmospheric environment. Three typical degraded image types are hazy, underwater, and sand-dust images. These three types of images have different color distributions. Many underwater image enhancement methods and some sand-dust image restoration approaches are based on ASM, which is a physical model for haze removal. The red channel prior [27], [28] and blue channel prior [25], [26] are frequently used in enhancing images. However, inverting the red or blue channel can over-enhance the red or blue components. Furthermore, the blue channel prior plays a role in reinforcing the weak blue component, but does not work to weaken the strong red component. Table 1 summarizes the color characteristics of degraded images.

Fig. 1 shows a single-sample hazy image, two underwater images and two sand-dust images with their atmospheric veils and histograms. As shown in Fig. 1(a), the hazy image has a gray veil, and its histogram shows similar red, green, and blue distributions. Underwater images have a weak red component with greenish (Fig. 1(b)) or bluish (Fig. 1(c)) veil depending on the intensity of the green component. In contrast, the sand-dust image presented in Fig. 1(d) has a yellow veil. This image has a weak blue component, normal green component, and strong red component. As shown in Fig. 1(e), the sand-dust image with both weak green and blue components has a reddish veil. As shown in Fig. 1, sand-dust images have strong red components as well as weak blue components. Therefore, we introduce an effective color balance algorithm that weakens the red component and strengthens the blue component to obtain a coincident chromatic histogram.

III. PROPOSED METHOD

The proposed method consists of four steps as follows.

- *Step 1:* Adaptive initial color correction.
- *Step 2:* Green mean-preserving color normalization technique.
- *Step 3:* Color pixel shifting based on maximum histogram overlapping.
- *Step 4:* Image adjustment for obtaining brighter image.

TABLE 1. Color characteristics of degraded images and undesired artifacts of restored images.

	Color characteristics			
Degrade image	Red	Green	Blue	Veil
Hazy	normal	normal	normal	gray
Underwater I	weak	normal	weaker than green	greenish
Underwater II	weak	weaker than blue	normal	bluish
Sand-dust I	strong	normal	weak	yellowish
Sand-dust II	strong	weak	weak	reddish

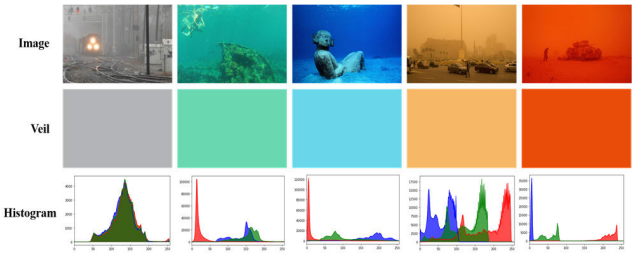

FIGURE 1. Degraded image sample with its veil and histogram. (a) Hazy image, (b) underwater image with greenish veil, (c) underwater image with bluish veil, (d) sand-dust image with yellowish veil, and (e) sand-dust image with reddish veil.

Overall, the proposed steps aim to obtain a coincident chromatic histogram. The goal of our method is to remove color veils due to sand dust, and to improve the brightness and contrast of the sand-dust image.

A. INITIAL COLOR CORRECTION

We use an initial color correction algorithm based on weighted green component compensation. Let $\mathbf{I}^c$ ($c \in \{r, g, b\}$) be the color channel of the given sand-dust image, and $I^c(\mathbf{x})$ be the pixel value of $\mathbf{I}^c$ at the position $\mathbf{x}= (x, y)$ within the image. The color correction is achieved as follows.

$$I_1^c(\mathbf{x}) = I^c(\mathbf{x}) + \Delta^c I^g(\mathbf{x}), \tag{1}$$

where $I_1^c(\mathbf{x})$ is a color-corrected pixel, and Δ^c is the weight of the green pixel. In this paper, we propose three factors to construct Δ^c. That is,

$$\Delta^c = \delta_{md}^c \times \delta_{sr}^c \times \delta_{wm}^c(\mathbf{x}), \tag{2}$$

where δ_{md}^c and δ_{sr}^c are global weighing factors based on the mean difference and standard deviation ratio, respectively. In (2), $\delta_{wm}^c(\mathbf{x})$ is the pixel-based local weighting factor that controls the amount of color correction by measuring the strength of a color pixel.

δ_{md}^c is the weight based on the mean difference, which is

$$\delta_{md}^c = m(\mathbf{I}^g) - m(\mathbf{I}^c), \tag{3}$$

where $m(\mathbf{I}^c)$ is the mean of $\mathbf{I}^c$. δ_{md}^c performs two color correction tasks. It determines the direction of the pixel correction. If $m(\mathbf{I}^c)$ is smaller than $m(\mathbf{I}^g)$, $\delta_{md}^c > 0$, thus, $I_1^c(\mathbf{x})$ is increased. Because a common sand-dust image has a weak blue component, almost all blue pixel values will increase. For the red component of the sand-dust image, $m(\mathbf{I}^c)$ is larger than $m(\mathbf{I}^g)$. Thus, the red color values decrease.

δ^c_{md} was successfully exploited in various white balance methods [29]–[31] for underwater image color correction. This factor plays an important role in various color-correction algorithms.

In our previous works, we presented an improved underwater color correction method using the standard deviation ratio of color channels [30], [31]. Although color channels have the same mean, their standard deviations can be different. Therefore, compensating for the color channel by considering only the difference in the mean is insufficient. δ^c_{sr} is a channel-dependent term that sufficiently compensates for the weak or strong color channel, which is defined as

$$\delta^c_{sr} = \frac{\sigma(\mathbf{I}^g)}{\sigma(\mathbf{I}^c)}, \tag{4}$$

where $\sigma(\cdot)$ is the standard deviation. In almost all sand-dust images, $\sigma(\mathbf{I}^g) > \sigma(\mathbf{I}^b)$ because the blue channel is weak. Therefore, the pixel values of the blue channel are sufficiently increased by δ^c_{sr}. The pixel values of the strong red component are adjusted according to $\sigma(\mathbf{I}^g)/\sigma(\mathbf{I}^r)$.

In underwater image enhancement approaches [29]–[31], the $1 - I^c(\mathbf{x})$ term is considered as a weakness measure of the color channel. For a weak red channel, because $I^r(\mathbf{x})$ is very small in an underwater image, $1 - I^r(\mathbf{x})$ is large enough to compensate for the weak red channel. In the case of the sand-dust image, the red channel is very strong, thus $1 - I^r(\mathbf{x})$ becomes too small to compensate for the strong red channel properly. For the same reason, $1 - I^b(\mathbf{x})$ for the blue channel can be so large that it can compensate for the blue channel excessively. In this paper, we propose a pixel-wise weight $\delta^c_{wm}(\mathbf{x})$, which is a generalized form of the weight used in the conventional method [29]. We define $\delta^c_{wm}(\mathbf{x})$ as follows.

$$\delta^c_{wm}(\mathbf{x}) = 1 - \kappa I^c(\mathbf{x}), \tag{5}$$

where κ is a control parameter. If κ is set to 1, $\delta^c_{wm}(\mathbf{x})$ is the same as that in the conventional underwater image color correction [29]. Because a sand-dust image has a weak blue channel and strong red channel, setting κ to 1 results in an excessive increase in the blue channel value and a small value change in the red channel. In this paper, we introduce κ, which is obtained by averaging the mean of the red channel and the mean of the inverted blue channel.

$$\kappa = \frac{\left(1 - m(\mathbf{I}^b)\right) + m(\mathbf{I}^r)}{2}. \tag{6}$$

As shown in (5), $\delta^c_{wm}(\mathbf{x})$ is a first-order equation with a negative slope of $-\kappa$. $\delta^c_{wm}(\mathbf{x})$ controls the amount of pixel change, and κ determines the range of the overall change. When $\delta^c_{sr} = 1$ and $\kappa = 1$, Δ^c becomes the same as that in the conventional underwater image color correction [29].

Fig. 2 shows the initial color correction result using the proposed method and the conventional approach. As shown in Fig. 2(b), both the mean and standard deviation of the red channel are changed to be negligible, that is, the mean is changed from 211.8 to 209.0, and the standard deviation is changed from 40.3 to 40.7. The mean and standard deviation of the blue channel are slightly strengthened. In contrast, we can see that the red channel is more weakened, and the blue channel is further strengthened as shown in Fig. 2(c). In conclusion, the proposed initial color correction step adjusts not only the mean but also the standard deviation more than the existing method. As shown in Fig. 2, the red component is still strong, and the blue color is still weak. The proposed pixel-based initial correction step slightly changes the color histograms. However, this initial correction step plays an important role in the next green-mean-preserving step.

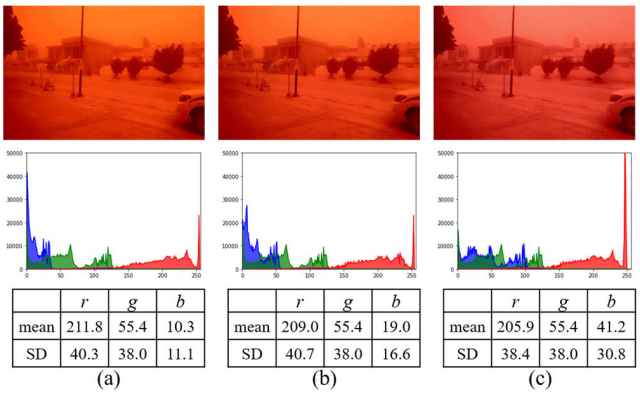

	r	g	b
mean	211.8	55.4	10.3
SD	40.3	38.0	11.1

(a)

	r	g	b
mean	209.0	55.4	19.0
SD	40.7	38.0	16.6

(b)

	r	g	b
mean	205.9	55.4	41.2
SD	38.4	38.0	30.8

(c)

FIGURE 2. Effect of proposed initial color correction and conventional method and their effect on final enhanced image. (a) Sand-dust image, (b) initial color correction result by conventional method [29], (c) initial color correction result by proposed method. In this Figure, SD means standard deviation.

B. GREEN-MEAN-PRESERVING IMAGE NORMALIZATION

The gray-world theory assumes that the average reflectance in a scene under a neutral light source is aromatic [9], [32]. According to this assumption, all the color values are nearly equivalent and the color in each channel averages to gray over the entire image. Therefore, to stretch color components according to the mean of the green component, we present a green-mean-preserving image normalization algorithm. This step is simple, but very effective. Let $I^c_2(\mathbf{x})$ be the normalized image, which is defined as

$$I^c_2(\mathbf{x}) = \frac{I^c_1(\mathbf{x}) - m\left(I^c_1(\mathbf{x})\right)}{\max_{\mathbf{x}} I^c_1(\mathbf{x}) - \min_{\mathbf{x}} I^c_1(\mathbf{x})} + m\left(I^g(\mathbf{x})\right). \tag{7}$$

From (7), we can easily verify that $m(\mathbf{I}^c_2) = m(\mathbf{I}^g)$. Using the image normalization process, the color veil of many sand-dust images can be removed. In addition, this process is affected by the previous initial color correction step.

Fig. 3 illustrates the results of the proposed green-mean-preserving image normalization method. The color veil due to the sand dust is almost removed as shown in Fig. 3. However, a minor color cast and low image brightness are still problematic and need to be addressed. Fig. 4 shows color correction results of Step 2 without Step 1. As shown in Fig. 4, severe color casts occur when applying the image normalization without the initial color correction step. From this result,

FIGURE 3. Intermediate color correction result based on Step 2 after Step 1.

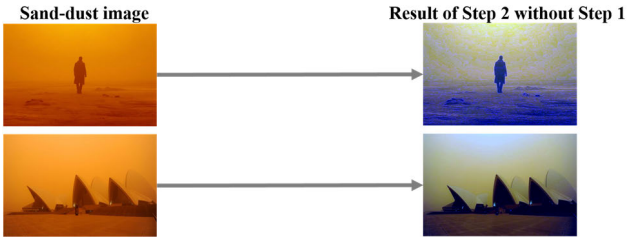

FIGURE 4. Intermediate color correction result based on Step 2 without Step 1.

strong or weak color components prevent the proper stretch of color values. This fact implies that the initial color correction, which weakens or strengthens color values in advance is important. In the next two steps, we remove the minor color cast and enhance the brightness of the color-corrected image.

C. COLOR PIXEL SHIFT BASED ON MAXIMUM HISTOGRAM OVERLAPPING

Because sand-dust images have a predominant color, such as red, the gray-world algorithm, which has the same color mean, can cause color casts. Fig. 5(a) presents the results of two sand-dust image samples after initial color correction and green-mean-preserving normalization. As shown in Fig. 5(a), the histogram of red channel is narrow and has a high peak. Because of the narrow and high-peak histogram, the processed image has a reddish artifact. This is caused by equating the red or blue mean to the green mean.

In this paper, we propose a color pixel shifting algorithm using the maximum histogram overlapping method as in Step 3. To avoid the effect of background luminance, we use normalized color values as follows.

$$I^c_{2,n}(\mathbf{x}) = \frac{I^c_2(\mathbf{x})}{\sum_c I^c_2(\mathbf{x})}, \tag{8}$$

where $I^c_{2,n}(\mathbf{x})$ is the normalized pixel value. Let $\mathbf{h}^c$ be the histogram function with 256 bins of $\mathbf{I}^c_{2,n}$, and $h^c(k)$ be the number of pixels with a value of k ($0 \le k \le 255$). Let $\mathbf{h}^c[\tau^c]$ be the histogram function shifted by the amount of τ^c ($-255 < \tau^c < 255$), where τ^c is the shifting index, and $h^c[\tau^c](k) = h^c(k + \tau^c)$. For example, $\mathbf{h}^c[0]$ is the original histogram from $\mathbf{I}^c_2\, n$, and $\mathbf{h}^r[-25]$ is the red channel histogram shifted by -25. Using the histogram shift, we can

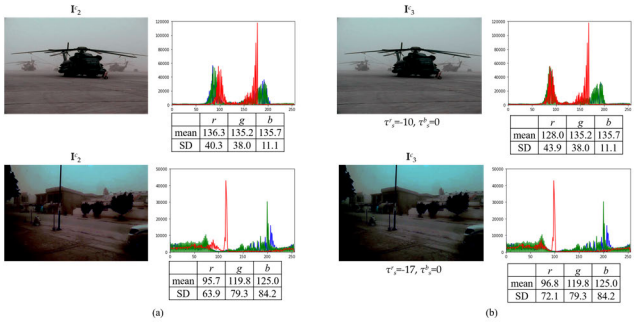

FIGURE 5. Intermediate results of Step 2 and Step 3. (a) Intermediate results of Step 2, and (b) intermediate results of Step 3 after applying Step 2.

achieve the maximum overlap of the three color channels. Let $H(\tau^r, \tau^g, \tau^b)$ be the histogram overlapping count, which is defined as

$$H(\tau^r, \tau^g, \tau^b) = \sum \#\left(\mathbf{h}^r[\tau^r] \cap \mathbf{h}^g[\tau^g] \cap \mathbf{h}^b[\tau^b]\right), \tag{9}$$

where $\#(\cdot)$ is the number of pixels. In this study, we let $\tau^g = 0$ to fix the green histogram. To find the maximum histogram overlap condition, we determine the shifting index using the maximum operation as follows.

$$\tau^r_s, \tau^b_s = \arg\max_{\tau^r, \tau^b} H(\tau^r, \tau^g = 0, \tau^b), \tag{10}$$

where τ^r_s and τ^b_s are the shifting index of the maximum histogram overlap for the red and blue components, respectively. By using τ^r_s and τ^b_s, we obtain $I^c_3(\mathbf{x})$ as follows.

$$I^c_3(\mathbf{x}) = I^c_2(\mathbf{x}) + \tau^c_s, \tag{11}$$

In this case, $\tau^g_s = 0$.

Fig. 5(b) shows two intermediate results of $\mathbf{I}^c_3$ after applying the proposed Step 3. As shown in Fig. 5(b), the reddish artifacts are removed. The mean of the top image of Fig. 5(b) is reduced (from 136.3 to 128.0), and its standard deviation is increased (from 40.3 to 43.9). Because the standard deviation increases, the distribution of the red component is wider. The standard deviation of the bottom image of Fig. 5(b) also increases from 63.9 to 72.1. Therefore, the narrow red channel distribution is expanded, resulting in the removal of the reddish artifact. From these examples, we can see the effectiveness of the proposed algorithm.

Fig. 6 presents more examples for considering the effectiveness of the proposed three steps. As shown in the top row image of Figure 6, the red components are reduced ($\tau^r_s = -3$). The third row image of Figure 6 has $\tau^r_s = -9$ and $\tau^b_s = 10$, so that the reddish effect is reduced while the blue effect is slightly increased. In conclusion, the proposed color shift using the maximum histogram overlapping can fine-tune the color cast.

D. FINAL IMAGE ADJUSTMENT

Because a significant amount of light is absorbed by sand-dust particles, many captured sand-dust images appear dark.

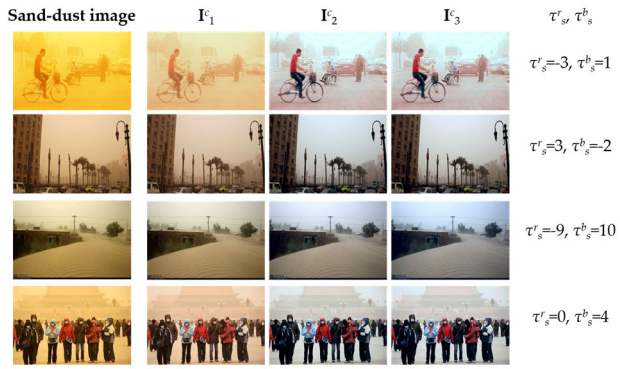

FIGURE 6. Intermediate result of I^c_3 by applying pixel shift based on maximum histogram overlapping.

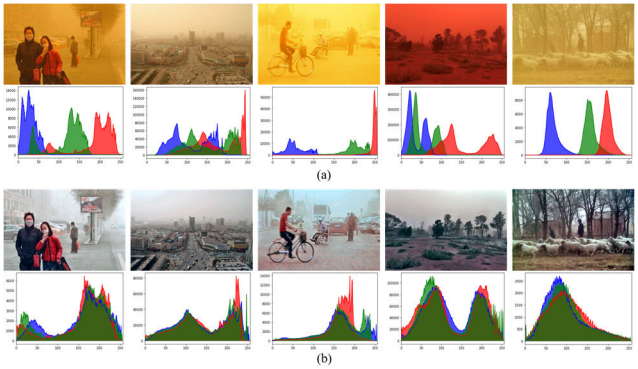

FIGURE 7. Sand-dust images and their restored versions. (a) Sand-dust images and corresponding histograms, and (b) enhanced images based the proposed algorithm.

Therefore, we finally exploit the well-known image adjustment algorithm as follows.

$$I^c_f(\mathbf{x}) = \frac{I^c_3(\mathbf{x}) - \min\limits_c \left(\min\limits_{\mathbf{x}} I^c_3(\mathbf{x})\right)}{\max\limits_c \left(\max\limits_{\mathbf{x}} I^c_3(\mathbf{x})\right) - \min\limits_c \left(\min\limits_{\mathbf{x}} I^c_3(\mathbf{x})\right)}, \quad (12)$$

where $I^c_f(\mathbf{x})$ corresponds to the final enhanced image. In this study, we drop color pixel values greater than 95.5% and less than 0.5%. The overall algorithm for sand-dust image enhancement in an image is presented in Table 2.

TABLE 2. Overall algorithm of the proposed method.

Input: Input image $\mathbf{I}$
Output: Enhanced image $\mathbf{I}_f$.
1) Obtain initial color corrected image $\mathbf{I}_1$ using (1).
2) Obtain normalized image $\mathbf{I}_2$ using (7).
3) Select shift index τ^r_s based on (10) and obtain mean shifted image $\mathbf{I}_3$ using (11).
4) Obtain the final enhanced image $\mathbf{I}_f$ using (12).

Fig. 7 shows various histograms of sample sand-dust images (Fig. 7(a)) and their enhanced images (Fig. 7(b)) by the proposed method. As shown in Fig. 7, restored sand-dust images obtained using the proposed algorithm have a nearly coincident chromatic histogram. The red and blue histograms tend to resemble the stretched green histogram. The coincident chromatic histogram can remove color veils caused by various types of sand-dust or red-storm. From Fig. 7, we can see that our approach effectively makes the chromatic histogram coincident.

E. EFFECT OF PROPOSED STEPS

We combine each of the presented four steps to generate five combinations, and examine the results to evaluate the effectiveness of the proposed sand-dust image enhancement method. The enhancement results are shown in Table 3.

- *Combination I:* Step 1 + Step 4

As shown in Table 3, we can see that proper image enhancement results cannot be obtained without Step 2 or

TABLE 3. Case study for various combination of proposed steps. five combinations are examined and discussed for verifying the effect of each step in the proposed enhancement algorithm.

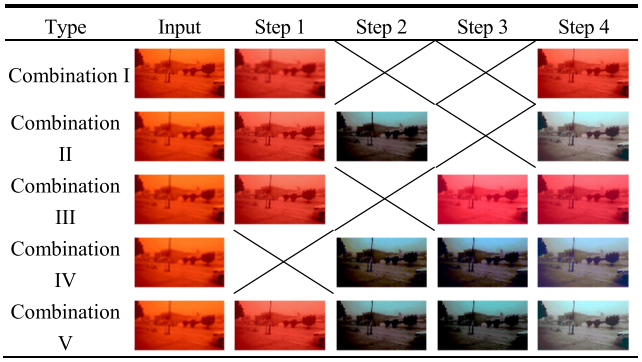

Step 3. In particular, the green-mean-preserving technique is a crucial step. Almost all color correction and white balance algorithms use the green information. Therefore, if green information is not used in any form, proper results cannot be obtained.

- *Combination II:* Step 1 + Step 2 + Step 4

By applying Step 1 and Step 2 successively, we can obtain a usable enhanced image. However, a minor color cast can occur as presented in Section III. C. In particular, if the sand-dust image has a very weak blue channel or a very strong red channel, this combination can cause a color cast.

- *Combination III:* Step 1 + Step 3 + Step 4

This combination does not generate good results because Step 2 is missing as in Combination I.

- *Combination IV:* Step 2 + Step 3 + Step 4

This combination shows the role of the proposed initial color-correction step. The color correction results obtained by including Step 1, Step 2, and Step 1 without initial color correction generate bluish images. This bluish result is due to the over-enhancement of a weak blue channel. The undesirable bluish artifact frequently appears in blue channel prior-based methods [25], [26] that invert the blue color component.

- *Combination V:* Step 1 + Step 2 + Step 3 + Step 4

FIGURE 8. Enhancement results of various sand-dust images with weak sand-dust veils.

This combination presents the proposed sand-dust image enhancement scheme. As shown in Table 3, this combination achieves the best enhancement performance.

However, the proposed sand-dust image enhancement algorithm cannot completely remove the red veil when the red histogram of the image has a very narrow peak at a high pixel value (see the results shown in Fig. 10). Our future research direction is to study a robust enhancement algorithm that can be applied well to red-storm images with a very narrow and high peak at a high pixel value.

FIGURE 9. Enhancement results of various sand-dust images with considerable amount of color veils.

IV. SIMULATION RESULTS

To verify the effectiveness of the proposed sand-dust image enhancement method, we tested it on various sand-dust images collected through the Internet, in total, we tested 245 images. The performance of our approach is compared with those of 5 state-of-the-art methods, namely, fusion-based enhancement (FBE) [13], visibility enhancement via tri-threshold fuzzy intensification operators (TFIO) [17], halo-reduced dark channel prior (HRDCP) [24], normalized Gamma transformation (NGT) [19], and saturation-based transmission map estimation (STME) [5]. The codes for 5 image enhancement methods were downloaded from their project sites, and the code of the proposed algorithm and sand-dust image dataset are available in [32].

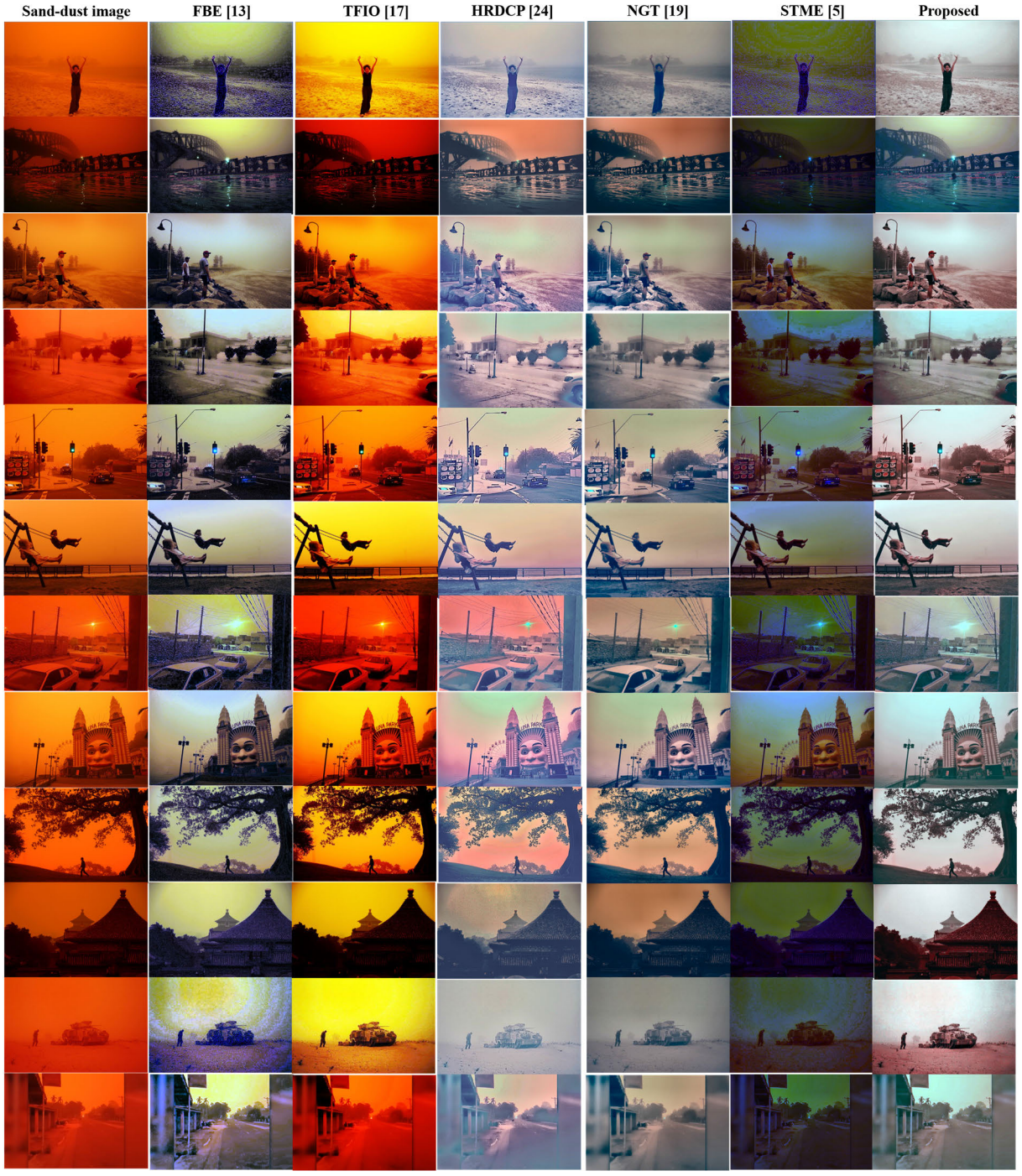

FIGURE 10. Enhancement results of various red-storm images with reddish sand-dust.

A. COMPUTATION TIME

The proposed method was implemented with an Intel i7-4790 CPU @ 3.60GHz and 8GB RAM without a multi-threading acceleration. The code was written in un-optimized Python in the Windows 10 environment. The existing methods to be compared were implemented in the same environment. The execution time was averaged over 20 execution times, and the times for reading and writing images were excluded. Table 4 presents the execution times for various image sizes. As summarized in Table 4, TFIO [17] and STME [5] achieve faster execution times than the proposed method for small images (500×422 and 1000×750). For larger images (2000×1091 and 4000×3000), the proposed scheme achieves the fastest execution time. The overall average execution time of our algorithm is the fastest as summarized in Table 4.

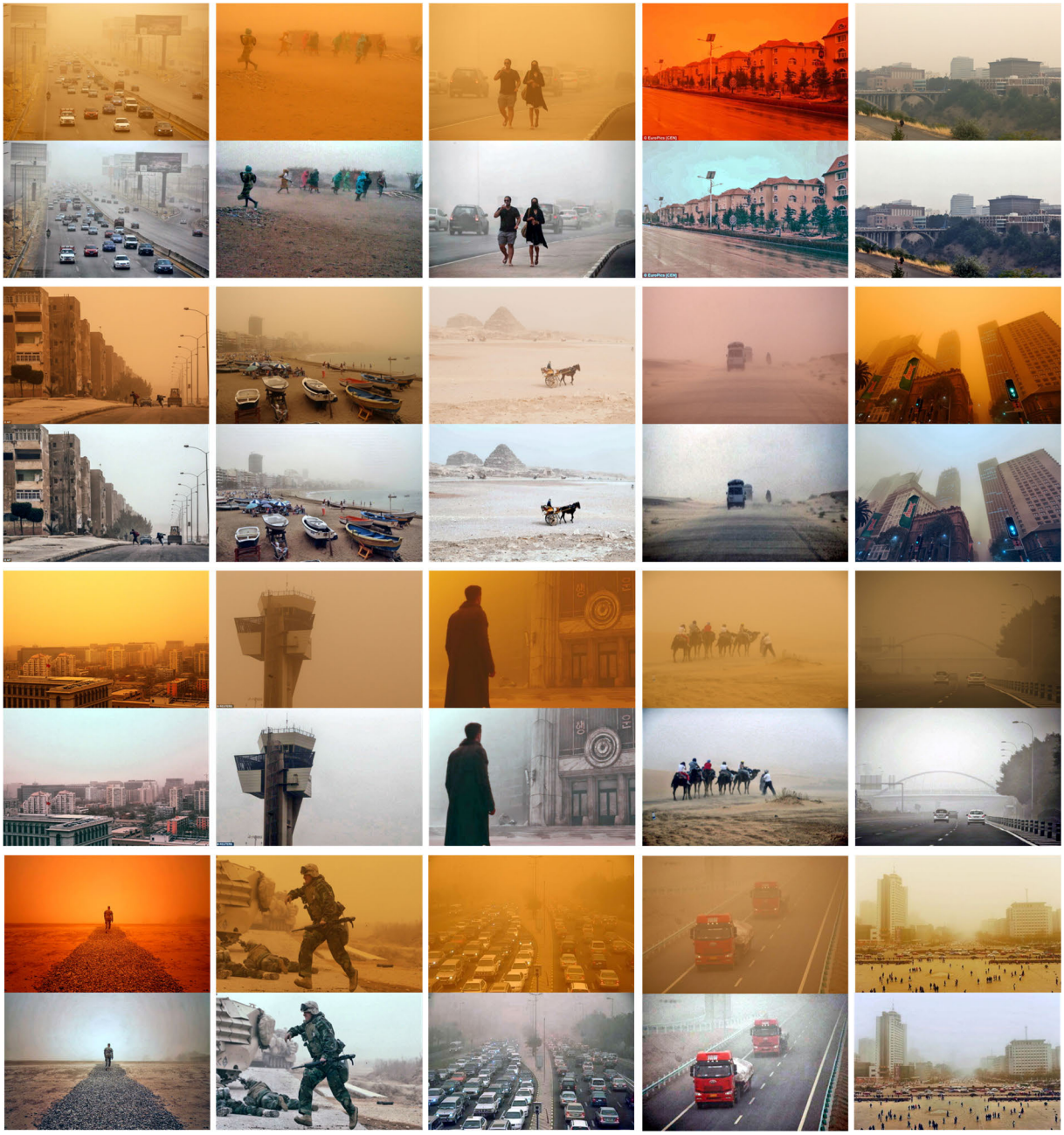

FIGURE 11. More sand-dust image enhancement results by the proposed method.

B. QUALITATIVE COMPARISION

In our simulation, we compare the proposed method with the existing methods for three types of sand-dust images, where the sand-dust veil is weak, significant, and heavy. We selected 12 representative images for each type from the test dataset and produced enhancement results for each method.

Fig. 8 shows a qualitative comparison of our results on weak sand-dust images with those of 5 state-of-the-art image enhancement methods. As shown in Fig. 8, TFIO [17] does not remove the color veils of sand-dust images. HRDCP [24] does not effectively enhance sand-dust images. Restored results obtained by this method have high contrast, however, they have color casts and dimmed colors, and look unnatural. STME [5], based on the gray-world assumption, sometimes fails to eliminate color veils and produces severe color casts. NGT [19] effectively removed sand-dust veils. Enhancement results based on NGT have low-contrast and dimmed colors in the images. FBE [13] generates reasonable restored images, which have little color cast, and veils are well removed. The proposed method shows the best qualitative results with high contrast, good brightness, and few color veils caused by sand-dust environment.

The enhancement results of sand-dust images with a considerable amount of color veils are presented in Fig. 9.

TABLE 4. Execution times of various algorithms (Unit: second).

Method	Image size				
	500×422	1000×750	2000×1091	4000×3000	Average
FBE [13]	0.765	1.459	3.465	17.560	5.815
TFIO [17]	0.101	0.427	2.803	25.914	14.061
HRDCP [24]	3.144	9.730	29.630	154.575	49.270
NGT [19]	0.343	0.631	1.386	6.821	2.293
STME [5]	0.094	0.356	1.104	6.886	2.110
Proposed	0.333	0.488	0.861	3.686	1.342

TFIO [17] fails to enhance sand-dust images, which are contaminated with a large amount of sand dust. HRDCP [24] and NGT [19] do not fully remove sand-dust veils and generate poorly enhanced images. Restored results obtained by STME [5] show severe bluish or yellowish artifacts. FBE [13], which can successfully be applied to weak sand-dust images, often fails to restore sand-dust images. Only the proposed approach generates reasonable results. Enhanced images obtained using the proposed method do not show any color casts and have high contrast and brightness.

Fig. 10 illustrates the enhancement results for nearly reddish sand-dust images, which can be called red-storm images. TFIO [17] cannot recover the sand-dust image at all, and causes a serious yellowish artifact. HRDCP [24] and NGT [19] are insufficient to properly restore red-storm images. In particular, these two methods fail to remove strong red components, thus images restored by these algorithms have yellowish pink veils. STME [5] always fails to recover sand-dust images with a heavy dust veil. The proposed method is not perfect for red-storm images, however, it enhances the degraded images to an appropriate level. Considering that the enhancement of the red-storm image is a very difficult task, the proposed algorithm is considered sufficiently applicable.

For a broader performance comparison, this paper presents the sand-dust image enhancement results for more than 20 test images in Fig. 11. A shown in Fig. 11, the enhancement results using the proposed algorithm are superior to those of other methods in terms of the restoration capability, detail recovery, and color shift. The advantages of the proposed method are significant when considering the computation time.

C. QUANTITATIVE COMPARISON

In the sand-dust image enhancement framework, the first important factor in evaluating image quality is the degree of removal of color veils caused by sand dust. However, there seems to be no quantitative quality evaluation measure for sand-dust images. Therefore, we exploit the non-reference underwater image quality measure (UIQM) [33], which is frequently used in the underwater image-enhancement field. Because UIQM evaluates the capability to remove color veils in enhancing underwater images, it can be used as a measure to evaluate the enhancement of sand-dust images. UIQM comprises three underwater image attribute measures: image colorfulness, image sharpness, and image contrast. A higher UIQM score is considered to yield a higher visual quality. Furthermore, 4 conventional non-reference quality measures, including the naturalness image quality evaluator (NIQE) [34], no-reference perception-based image quality evaluator (PIQUE) [35], blind/referenceless image spatial quality evaluator (BRISQUE) [36], and no-reference image quality metric for contrast distortion (NIQMC) [37], were tested. For NIQE, PIQUE, and BRISQUE, smaller values represent better image qualities, and for NIQMC, larger values indicate better qualities of the enhanced image.

Table 5 summarizes the comparison of 5 average quantitative measure values for all 245 test images. The top two performances are indicated in bold and italic. The proposed algorithm has the best average UIQM score. STME has the second-best UIQM score despite severe color distortion. FBE, TFIO, HRDCP, and NGT achieve UIQM scores similar to the subjective image qualities shown in Figures 8, 9, and 10. For NIQE, PIQUE, and BRISQUE scores, our method achieved the best average values followed by STME. As shown in Table 5, the highest NIQMC scores were obtained by the proposed algorithm and FBE. The NIQMC assesses image quality by measuring the local details and global histogram of the given image, and it particularly favors images with higher contrast. Meanwhile, STME obtains the lowest NIQMC score. In conclusion, the proposed method has the best performance when considering the scores of 5 quantitative measures. Therefore, the proposed enhancement scheme can generate more colorful images with a high contrast from UIQM perspective, and can produce more natural enhanced images comparing NIQE scores. In addition, we can judge that our method has less contrast distortion than other methods from the result of comparing the NIQMC values.

TABLE 5. Average quantitative metric values for 245 test images.

Method	Quantitative metrics				
	UIQM↑	NIQE↓	PIQUE↓	BRISQUE↓	NIQMC↑
FBE [13]	0.617	3.741	47.854	34.748	*5.450*
TFIO [17]	0.529	3.474	46.255	36.538	5.071
HRDCP [24]	0.593	4.123	46.111	32.034	4.786
NGT [19]	0.631	3.525	47.582	34.565	4.626
STME [5]	*0.653*	*3.456*	*45.300*	*31.325*	4.414
Proposed	**0.658**	**3.442**	**43.554**	**28.829**	**5.476**

V. CONCLUSION

In this paper, we proposed an efficient sand-dust image enhancement algorithm using a successive color balance to obtain a coincident chromatic histogram. We first introduced a color correction method based on the mean and standard deviation of color histograms. Second, a green-mean-preserving color normalization was presented to make the red and blue histograms resemble the green histogram. However, this process could result in an undesirable output because the red or blue components of many sand-dust images have a narrow histogram with a high peak. To tackle this problem, we proposed a histogram shifting method that makes the red and blue histograms overlap the green histogram as much as possible. Finally, image adjustment was applied to improve the brightness of the sand-dust image. The performance of

the proposed method was compared with those of existing sand-dust image enhancement algorithms. The simulation results showed that the proposed enhancement scheme outperforms state-of-the-art approaches in terms of both subjective and objective qualities.

REFERENCES

[1] K. He, J. Sun, and X. Tang, "Single image haze removal using dark channel prior," *IEEE Trans. Pattern Anal. Mach. Intell.*, vol. 33, no. 12, pp. 2341–2353, Dec. 2011.
[2] Q. Zhu, J. Mai, and L. Shao, "A fast single image haze removal algorithm using color attenuation prior," *IEEE Trans. Image Process.*, vol. 24, no. 11, pp. 3522–3533, Nov. 2015.
[3] B. Cai, X. Xu, K. Jia, C. Qing, and D. Tao, "DehazeNet: An end-to-end system for single image haze removal," *IEEE Trans. Image Process.*, vol. 25, no. 11, pp. 5187–5198, Nov. 2016.
[4] Z. Gu, Z. Zhan, Q. Yuan, and L. Yan, "Single remote sensing image dehazing using a prior-based dense attentive network," *Remote Sens.*, vol. 11, no. 24, p. 3008, Dec. 2019.
[5] S. E. Kim, T. H. Park, and I. K. Eom, "Fast single image dehazing using saturation based transmission map estimation," *IEEE Trans. Image Process.*, vol. 29, pp. 1985–1998, 2020.
[6] D. Berman, T. Treibitz, and S. Avidan, "Single image dehazing using haze-lines," *IEEE Trans. Pattern Anal. Mach. Intell.*, vol. 42, no. 3, pp. 720–734, Mar. 2020.
[7] Q. Bu, J. Luo, K. Ma, H. Feng, and J. Feng, "An enhanced pix2pix dehazing network with guided filter layer," *Appl. Sci.*, vol. 10, no. 17, p. 5898, Aug. 2020.
[8] N. Middleton, P. Tozer, and B. Tozer, "Sand and dust storms: Underrated natural hazards," *Disasters*, vol. 43, no. 2, pp. 390–409, Apr. 2019.
[9] G. Buchsbaum, "A spatial processor model for object colour perception," *J. Franklin Inst.*, vol. 310, no. 1, pp. 1–26, Jul. 1980.
[10] E. H. Land, "The retinex theory of color vision," *Sci. Amer.*, vol. 237, no. 6, pp. 108–129, Dec. 1977.
[11] J. van de Weijer, T. Gevers, and A. Gijsenij, "Edge-based color constancy," *IEEE Trans. Image Process.*, vol. 16, no. 9, pp. 2207–2214, Sep. 2007.
[12] C. Liu, X. Chen, and Y. Wu, "Modified grey world method to detect and restore colour cast images," *IET Image Process.*, vol. 13, no. 7, pp. 1090–1096, May 2019.
[13] X. Fu, Y. Huang, D. Zeng, X.-P. Zhang, and X. Ding, "A fusion-based enhancing approach for single sandstorm image," in *Proc. IEEE 16th Int. Workshop Multimedia Signal Process. (MMSP)*, Jakarta, Indonesia, Sep. 2014, pp. 1–5.
[14] T. Yan, L. Wang, and J. Wang, "Method to enhance degraded image in dust environment," *J. Softw.*, vol. 9, no. 10, pp. 2672–2677, Oct. 2014.
[15] S. K. Pal and R. A. King, "Image enhancement using smoothing with fuzzy sets," *IEEE Trans. Syst., Man, Cybern.*, vol. SMC-11, no. 7, pp. 494–501, Jul. 1981.
[16] J.-Y. Kim, L.-S. Kim, and S.-H. Hwang, "An advanced contrast enhancement using partially overlapped sub-block histogram equalization," *IEEE Trans. Circuits Syst. Video Technol.*, vol. 11, no. 4, pp. 475–484, Apr. 2001.
[17] Z. Al-Ameen, "Visibility enhancement for images captured in dusty weather via tuned tri-threshold fuzzy intensification operators," *Int. J. Intell. Syst. Appl.*, vol. 8, no. 8, pp. 10–17, Aug. 2016.
[18] J. Wang, Y. Pang, Y. He, and C. Liu, "Enhancement for dust-sand storm images," in *Proc. Int. Conf. Multimedia Modeling*, Miami, FL, USA, Jun. 2016, pp. 842–849.
[19] Z. Shi, Y. Feng, M. Zhao, E. Zhang, and L. He, "Normalised gamma transformation-based contrast-limited adaptive histogram equalisation with colour correction for sand–dust image enhancement," *IET Image Process.*, vol. 14, no. 4, pp. 747–756, Mar. 2020.
[20] A. M. Reza, "Realization of the contrast limited adaptive histogram equalization (CLAHE) for real-time image enhancement," *J. VLSI Signal Process.-Syst. Signal, Image, Video Technol.*, vol. 38, no. 1, pp. 35–44, Aug. 2004.
[21] S. G. Narasimhan and S. K. Nayar, "Vision and the atmosphere," *Int. J. Comput. Vis.*, vol. 48, no. 3, pp. 233–254, Jul. 2002.
[22] S.-C. Huang, J.-H. Ye, and B.-H. Chen, "An advanced single-image visibility restoration algorithm for real-world hazy scenes," *IEEE Trans. Ind. Electron.*, vol. 62, no. 5, pp. 2962–2972, May 2015.
[23] S. Yu, H. Zhu, J. Wang, Z. Fu, S. Xue, and H. Shi, "Single sand-dust image restoration using information loss constraint," *J. Mod. Opt.*, vol. 63, no. 21, pp. 2121–2130, Nov. 2016.
[24] Z. Shi, Y. Feng, M. Zhao, E. Zhang, and L. He, "Let you see in sand dust weather: A method based on halo-reduced dark channel prior dehazing for sand-dust image enhancement," *IEEE Access*, vol. 7, pp. 116722–116733, 2019.
[25] G. Gao, H. Lai, Z. Jia, Y. Liu, and Y. Wang, "Sand-dust image restoration based on reversing the blue channel prior," *IEEE Photon. J.*, vol. 12, no. 2, pp. 1–16, Apr. 2020.
[26] Y. Cheng, Z. Jia, H. Lai, J. Yang, and N. K. Kasabov, "Blue channel and fusion for sandstorm image enhancement," *IEEE Access*, vol. 8, pp. 66931–66940, Apr. 2020.
[27] C. Li, J. Quo, Y. Pang, S. Chen, and J. Wang, "Single underwater image restoration by blue-green channels dehazing and red channel correction," in *Proc. IEEE Int. Conf. Acoust., Speech Signal Process. (ICASSP)*, Shanghai, China, Mar. 2016, pp. 1731–1735.
[28] A. Galdran, D. Pardo, A. Picón, and A. Alvarez-Gila, "Automatic red-channel underwater image restoration," *J. Vis. Commun. Image Represent.*, vol. 26, pp. 132–145, Jan. 2015.
[29] C. O. Ancuti, C. Ancuti, C. De Vleeschouwer, and P. Bekaert, "Color balance and fusion for underwater image enhancement," *IEEE Trans. Image Process.*, vol. 27, no. 1, pp. 379–393, Jan. 2018.
[30] H. S. Lee, S. W. Moon, and I. K. Eom, "Underwater image enhancement using successive color correction and superpixel dark channel prior," *Symmetry*, vol. 12, no. 8, p. 1220, Jul. 2020.
[31] S. W. Moon, H. S. Lee, and I. K. Eom, "Improvement of underwater colour correction using standard deviation ratio," *Electron. Lett.*, vol. 56, no. 20, pp. 1051–1054, Aug. 2020.
[32] *Source Code for the Proposed Method and Sand-Dust Image Dataset*. Accessed: Nov. 24, 2020. [Online]. Available: https://sites.google.com/view/ispl-pnu/
[33] K. Panetta, C. Gao, and S. Agaian, "Human-visual-system-inspired underwater image quality measures," *IEEE J. Ocean. Eng.*, vol. 41, no. 3, pp. 541–551, Jul. 2016.
[34] A. Mittal, R. Soundararajan, and A. C. Bovik, "Making a 'completely blind' image quality analyzer," *IEEE Signal Process. Lett.*, vol. 20, no. 3, pp. 209–212, Mar. 2013.
[35] N. Venkatanath, D. Praneeth, M. C. Bh, S. S. Channappayya, and S. S. Medasani, "Blind image quality evaluation using perception based features," in *Proc. 21st Nat. Conf. Commun. (NCC)*, Mumbai, India, Feb. 2015, pp. 1–6.
[36] A. Mittal, A. K. Moorthy, and A. C. Bovik, "No-reference image quality assessment in the spatial domain," *IEEE Trans. Image Process.*, vol. 21, no. 12, pp. 4695–4708, Dec. 2012.
[37] K. Gu, W. Lin, G. Zhai, X. Yang, W. Zhang, and C. W. Chen, "No-reference quality metric of contrast-distorted images based on information maximization," *IEEE Trans. Cybern.*, vol. 47, no. 12, pp. 4559–4565, Dec. 2017.

TAE HEE PARK received the B.S. and M.S. degrees in electronics engineering from Pukyong National University, South Korea, in 1993 and 1996, respectively, and the Ph.D. degree in electronics engineering from Pusan National University, South Korea, in 2011. She is currently an Assistant Professor with the School of Mechatronics Engineering, Tongmyong University, South Korea. Her research interests include image processing, computer vision, and image forensics.

IL KYU EOM received the B.S., M.S., and Ph.D. degrees from the Department of Electronics Engineering, Pusan National University, South Korea, in 1990, 1992, and 1998, respectively. From 1997 to 2005, he was a Faculty Member with Miryang National University, South Korea. He has been on the Faculty with Pusan National University, since 2006. He is currently a Full Professor with the Department of Electronics Engineering, Pusan National University. His research interests include image processing, computer vision, digital image forensic, and machine learning.